Investigation and improvement of sensitivity computation using the area-fraction weighted fixed grid FEM and structural optimization

Peter D Dunning[a,*], H Alicia Kim[a], Glen Mullineux[a]
[a]Department of Mechanical Engineering, University of Bath, Bath, UK

ABSTRACT

Boundary based structural optimization methods often employ a fixed grid FEM to compute sensitivities for efficiency and simplicity. A simple and popular fixed grid approach is to modify the stiffness of elements intersected by the boundary by an area-fraction weighting. However, poor sensitivities and numerical instabilities can occur when using this method. Sensitivity computation for a compliance objective is investigated and the results are used to develop a weighted least squares scheme to improve sensitivities computed by the area-fraction approach. This is implemented together with a numerically stable structural topology optimization using the level set method with no additional filtering or regularization. The performance of the proposed scheme is demonstrated by classic benchmark examples of topology optimization.

Keywords: Fixed grid; Area-fraction weighting; Sensitivity computation; Least squares method; Level set method; Structural topology optimization.

[*] Corresponding author. Tel.: +44 (0) 1225 385138
E-mail address: P.D.Dunning@bath.ac.uk

1. Introduction

The fixed grid Finite Element Method (FEM) is often employed in boundary based structural topology optimization methods to compute response states and sensitivities [1,2,3,4,5]. This Eulerian approach avoids re-meshing and hence is suitable for iterative boundary modifications in structural optimization [1,2,3,6]. However, this leads to fixed grid elements that are intersected by the boundary, which therefore possess discontinuous properties. Including elements with discontinuous properties in the analysis poses a challenge.

Various techniques have been employed in boundary based optimization to approximate the behaviour of the intersected elements. These include the extended FEM, which mimics the discontinuity by enriching shape functions by a Heaviside step function [7]. The Heaviside function is also sometimes approximated by a smooth function [8,9] when solving the linear elastic equation. The superimposed FEM fits a local mesh of flexible linear triangular elements to the boundary [6]. The local mesh is then coupled with the global fixed mesh during integration using a double mapping scheme. Another technique for improving the stiffness approximation of intersected elements is through fitting shape functions to the boundary and using degenerate elements [2].

Boundary based structural optimization methods are iterative and can require a large number of analyses during the optimization process. It is well known that the greatest computational burden in this type of structural optimization is the FE analysis step, thus the simpler and more efficient approach of the area-fraction approach is still popular. This simple approach is to weight the stiffness of intersected elements by the area-fraction of structural material within the element, or volume-fraction in three

dimensions. The Area-fraction weighted Fixed Grid (AFG) approach has been employed by spline based optimization methods [3,10] and the increasingly popular level set based methods [1,11,12]. The area-fraction approach is sometimes referred to as the "ersatz" material approach, where the non-structural regions within the fixed mesh are filled with a fictitious weak material. This is equivalent to the AFG method when stiffness of the weak material is significantly lower than that of the structural material.

Boundary based structural optimization methods often rely on shape sensitivities computed along the boundary to derive a velocity function that is used to propagate the design towards an optimum [1,6,8,11]. Therefore, the optimum shape of the structure is determined by the sensitivity distribution along the boundaries. The accuracy of the sensitivity distribution, in particular, the "relative" sensitivity values are important for structural optimization and the "absolute" accuracy of sensitivity is perhaps less critical [6,8,11]. The relative accuracy can also be characterized by a constant distribution of errors. A non-constant distribution of errors can fundamentally change the minimizing direction of an optimizer and the iterative nature of optimization can exacerbate the error and lead to destabilizing the optimization or even to non-convergence. This importance of the relative accuracy of sensitivity is a distinct characteristic for boundary based structural optimization in contrast to the FE studies for general analysis and this is the area we aim to focus on in this paper.

The destabilizing effects of the AFG method due to the distribution of boundary sensitivities and velocities have been observed by a number of researchers [2,6]. It is therefore common to smooth or regularize the velocity function to avoid numerical problems and improve reliability of convergence. For example the velocity function can

be smoothed across the boundary discontinuity using a simple linear filter [11], or it can be regularized by including a term dependent on mean curvature [12]. However, these smoothing techniques do not address the fundamental problem of poor sensitivity computation by the AFG method and introduce additional numerical parameters which influence optimum solutions. The selection of these parameters is often problem-dependent and can be difficult. These additional schemes may not be required if an accurate and smooth distribution of boundary sensitivities is computed directly from the fixed grid FEM. This can have an advantage of improving optimization convergence and computational efficiency.

The purpose of this paper is to investigate reasons for poor sensitivity computation when using the AFG method and present an improved numerical strategy for boundary sensitivity computation. The investigation is undertaken in the context of the classic minimization of total compliance problem, which has been widely studied in structural topology optimization [1,4,6,9]. This leads to a numerical strategy for boundary sensitivity distribution using a weighted least squares approach suitable for general boundary based optimization methods. The paper then presents a level set based topology optimization implementation with stable numerical properties and the improved scheme is demonstrated using classic benchmark examples from structural topology optimization.

2. Structural optimization for compliance using the level set method

This section introduces the minimization of compliance structural optimization problem and briefly reviews how the problem can be solved using the level set method.

First the structure is defined by an implicit function $\varphi(x)$, so that its zero level set coincides with the boundary:

$$\begin{cases} \varphi(x) > 0, & x \in \Omega_S \\ \varphi(x) = 0, & x \in \Gamma_S \\ \varphi(x) < 0, & x \notin \Omega_S \end{cases} \tag{1}$$

where Ω_S is the domain of the structure and Γ_S is the boundary of the structure. The compliance of the structure, $C(u, \varphi)$ is minimized subject to an upper limit on structural volume:

$$\begin{aligned} &\text{Minimize}: C(u,\varphi) = \int_\Omega \bar{E}_{ijkl}\varepsilon(u)_{ij}\varepsilon(u)_{kl} H(\varphi(x))d\Omega \\ &\text{Subject to}: \int_\Omega H(\varphi(x))d\Omega \le Vol^* \end{aligned} \tag{2}$$

where Vol^* is the upper limit on volume, $\bar{E}$ is the material property tensor, $\varepsilon(u)$ the strain tensor under displacement field u and Ω the domain of the fixed grid, such that $\Omega_S \subset \Omega$, and $H(x)$ is the Heaviside step function:

$$H\big(\varphi(x)\big) = \begin{cases} 1, & \varphi(x) \ge 0 \\ 0, & \varphi(x) < 0 \end{cases} \tag{3}$$

Boundary based optimization methods often use shape sensitivities computed along the boundary to move the design towards an optimum. For a homogenous linear elastic structure, if there are no body forces acting on the structure, the shape derivative of the compliance objective is [1]:

$$C'(u,\varphi) = \int_{\Gamma_o} \varsigma(u) V_n d\Gamma_0 \tag{4}$$

$$\varsigma(u) = \bar{E}_{ijkl}\varepsilon(u)_{ij}\varepsilon(u)_{kl} \tag{5}$$

where $\varsigma(u)$ is the sensitivity of the compliance objective, Γ_0 is the portion of Γ_S that is free of boundary conditions and V_n is a velocity function normal to the boundary, defined

such that a positive value indicates inward movement. The velocity function can be simply defined to reduce the objective [1]:

$$V_n = \lambda - \varsigma(u) \tag{6}$$

where λ is used to enforce the volume constraint and can be either fixed [1] or updated during the optimization [11]. The level set optimization method updates the structure by propagating the implicit function, Eq. (1) using the velocity function, Eq. (6) by solving a discretized Hamilton-Jacobi type equation [1,8]:

$$\varphi_i^{k+1} = \varphi_i^k - \Delta t V_{n,i} \left| \nabla \varphi_i^k \right| \tag{7}$$

where i is a discrete grid point, k is the current iteration and Δt is the time step defined by the Courant–Friedrichs–Lewy (CFL) condition for stability:

$$\Delta t = \beta h / \left| V_n \right|_{\max} \tag{8}$$

where h is the grid spacing and $0 < \beta < 1$.

The velocity function used to update the design is computed directly from boundary shape sensitivities, $\varsigma(u)$. For practical problems, sensitivities are determined numerically from the stress and strain fields using a fixed grid FEM. Thus, the relative accuracy and smoothness of the fixed grid stress and strain fields directly affects the optimization of the structure and the final solution obtained.

3. AFG element sensitivity investigation

The AFG method approximates the stiffness of intersected elements using a simple area-fraction weighting. Boundary sensitivities for a compliance objective function are then computed by the product of stress and strain, Eq. (5) and directly used to determine boundary velocities, Eq. (6).

When using the AFG method to analyse a simple structure, it has been shown that maximum displacement errors occur at the structure boundary where intersected elements exist [13]. This produces stress errors that are also greatest at the boundary and maximum at stress concentrations. Furthermore, stresses computed by nodal averaging are not guaranteed to converge in the limit of mesh refinement [13]. This suggests that errors in boundary sensitivity Eq. (5), and also velocity, Eq. (6) are greatest along the boundary where intersected elements are present. Furthermore, stress errors can be caused by the discontinuity of material properties between interior and intersected elements [14].

We investigate the effects of intersected element stiffness approximation on sensitivity by computing stress, strain and sensitivity values for an abstract AFG element using a set of simple loading conditions. The AFG method in 2-d approximates an intersected element by reducing its stiffness to αE, where E is the modulus of the real material and α is the area-fraction of material within the element. This effectively homogenizes the fixed grid element, as its dimensions remain the same, but its stiffness is reduced. Displacements are computed in the usual way at the nodes, some of which lie outside the structure. The displacement field of this fictitiously enlarged element is used to obtain the stress, strain and hence sensitivity for structural optimization.

The following sections compare the approximated sensitivity values of a rectangular shape material within a homogenized square fixed grid element (Fig. 1a) to exact values calculated using a fitted element.

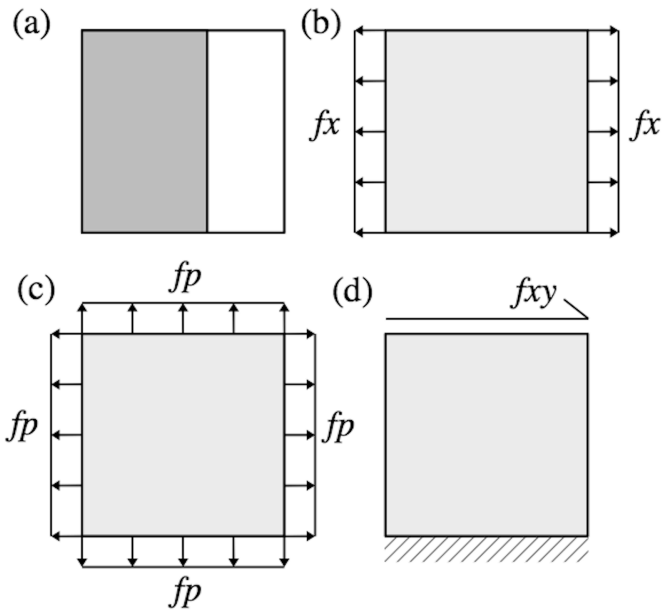

Fig. 1. (a) Abstract element; (b) uniaxial loading; (c) biaxial loading; (d) shear loading

The relative error between approximated and exact sensitivities is computed by:

$$\eta(\varsigma) = \left|\varsigma - \varsigma_{AFG}\right| / \varsigma \tag{9}$$

where ς is computed by Eq. (5), using the equivalent rectangular element and real Young's modulus, E. ς_{AFG} is computed using a square element ($h \times h$) and approximated stiffness, αE. Three simple loading conditions, Fig. 1b-d are considered in the study.

3.1 Uniaxial Loading

Stress, strain and sensitivity values are calculated for elements subject to uniaxial loading, Fig.1b. Relative error in sensitivity, Eq. (9) is calculated by considering two rectangular shape materials $\alpha h \times h$ and $h \times \alpha h$. The calculations are summarised in Table 1 and show that relative error in sensitivity value increases as α decreases. Also, when

comparing the errors, $\eta(\varsigma)$ between the two rectangular materials, $\alpha h \times h$ and $h \times \alpha h$ it is apparent that errors are also dependent on the shape of the material within an element.

Table 1. Uniaxial loading, sensitivity relative error calculation summary.

Modulus	**Dimensions**	**Stress (σ_{xx})**	**Strain (ε_{xx})**	**ς ($\sigma_{xx} \times \varepsilon_{xx}$)**	**$\eta(\varsigma)$**
αE	$h \times h$	fx/h	$fx/\alpha Eh$	$fx^2/\alpha Eh^2$	-
E	$\alpha h \times h$	fx/h	fx/Eh	fx^2/Eh^2	$(1-\alpha)/\alpha$
	$h \times \alpha h$	$fx/\alpha h$	$fx/\alpha Eh$	$fx^2/\alpha^2 Eh^2$	$1-\alpha$

3.2 Biaxial loading

Stress, strain and sensitivity values are calculated for elements under biaxial loading, Fig.1c. In calculating the strain values the plane stress assumption is adopted, although similar results are obtained using plane strain. The calculations are summarised in Table 2 and show that for Poisson's ratio values, $v < 1$, the relative error in sensitivity, Eq. (9) increases as α decreases. However, the magnitude of the error is dependent on Poisson's ratio.

Table 2. Biaxial loading, sensitivity relative error calculation summary.

Modulus	**Dimensions**	**Stress (σ)**	**Strain (ε)**	**ς ($\sigma \times \varepsilon$)**	**$\eta(\varsigma)$**
αE	$h \times h$	$\sigma_{xx} = fp/h$ $\sigma_{yy} = fp/h$	$\varepsilon_{xx} = \varepsilon_{yy} =$ $(1-v)(fp/\alpha Eh)$	$2(1-v)\times$ $(fp^2/\alpha Eh^2)$	-
E	$\alpha h \times h$	$\sigma_{xx} = fp/h$ $\sigma_{yy} = fp/\alpha h$	$\varepsilon_{xx} = (\alpha-v)(fp/\alpha Eh)$ $\varepsilon_{yy} = (1-\alpha v)(fp/\alpha Eh)$	$(\alpha^2-2\alpha v+1)\times$ $(fp^2/\alpha^2 Eh^2)$	$(1+\alpha^2-2\alpha)/$ $(1+\alpha^2-2\alpha v)$

3.3 Shear loading

The shear modulus, G is directly proportional to Young's Modulus, therefore, the shear modulus using the area-fraction approximation is αG. The stress, strain and sensitivity values are calculated for elements subject to a shear load, Fig.1d. Relative error in sensitivity, Eq. (9) is calculated between an approximated element and two fitted rectangular elements $\alpha h \times h$ and $h \times \alpha h$, Table 3. For both cases the relative error in sensitivity value increases as α decreases, although the magnitude of the error is again dependent on the real geometry being approximated by the area-fraction weighting.

Table 3. Shear loading, sensitivity relative error calculation summary.

Shear Modulus	**Dimensions**	**Stress (σ_{xy})**	**Strain (ε_{xy})**	**ς ($\sigma_{xy} \times \varepsilon_{xy}$)**	**$\eta(\varsigma)$**
αG	$h \times h$	fxy/h	$fxy/\alpha Gh$	$fxy^2/\alpha Gh^2$	-
G	$\alpha h \times h$	$fxy/\alpha h$	$fxy/\alpha Gh$	$fxy^2/\alpha^2 Gh^2$	$1 - \alpha$
	$h \times \alpha h$	fxy/h	fxy/Gh	fxy^2/Gh^2	$(1 - \alpha)/\alpha$

3.4 Discussion

For all examples and loading conditions considered above, the relative error in sensitivities increases as α decreases. In addition, the magnitude of the error can depend on the geometry of the material shape, as for the uniaxial and shear loading cases, and also on Poisson's ratio as for the biaxial loading case. This suggests that boundary sensitivity and velocity distribution between neighbouring elements with significantly different α values may not be smooth, as errors depend on the shape and size of the materials being approximated by the AFG formulation. Local roughness in the velocity function due to varying error in sensitivity computation can produce a spuriously rough

boundary during the design update. In addition, the inconsistent errors in successive iterations can exacerbate this effect. This phenomenon can lead to a non-optimal solution or even to non-convergence.

4. Improvement of AFG sensitivity computation

We investigate methods for computing boundary sensitivities using the AFG method. The lower order elements commonly employed in structural optimization do not usually enforce inter-element continuity of gradient fields, such as the strain and stress fields used to compute boundary sensitivities, Eq. (5). Common methods for computing gradient fields in FEA are to average element values at nodes and then interpolate using element shape functions, or to compute values at points within each element, then interpolate the sampled values using the least squares method [15]. In the context of boundary based optimization, the relative distribution of sensitivities and not their exact values is important. This is because the velocity function, Eq. (6) is usually normalized to meet the CFL stability condition [6,8]. Therefore, in the investigation, boundary sensitivities are divided by the absolute maximum value to produce a distribution of normalized velocities.

For all examples, a fitted mesh is also constructed using four node bilinear elements of similar sizes to those used for the fixed mesh. Normalized velocities are computed for the fitted mesh solution using the simple nodal averaging technique. The normalized velocity distribution computed from the fitted mesh provides a reasonable reference solution with which to compare the AFG results.

4,1 Nodal averaging methods

Normalized velocity distributions are computed using the simple nodal averaging technique and a weighted nodal averaging method, where the relative contribution of each element sensitivity value is weighted by its area-fraction:

$$V_{n,i} = \left(\sum_{j=1}^{n} \alpha_j V_{n,j} \right) / \sum_{j=1}^{n} \alpha_j \qquad (10)$$

where i denotes a point between elements where averaging occurs and j denotes an element with an edge coincident with point i.

4.2 Weighted least squares method

There are various parameters involved in employing a weighted least squares method. Firstly, the sampled data is fitted to a model, which usually takes the form of a basis function and our investigation found that a second degree polynomial provides sufficient accuracy for the sensitivity distribution in two dimensions:

$$\varsigma(x, y) = c_0 + c_1 x + c_2 y + c_3 xy + c_4 x^2 + c_5 y^2 \qquad (11)$$

where c_i are the unknowns computed by the least squares fitting process.

We apply the least squares method locally to compute sensitivity values at points along the boundary. This local approach uses only a subset of the sampled data points within a specific support radius. The support radius must be large enough to include at least six points to perform the least squares fit for Eq. (11).

Section 3 demonstrates that error in sensitivity computation increases as the area-fraction of the element decreases. We therefore propose to weight sampled sensitivity values by their associated area-fraction, $\langle$. This is in addition to weighting sampled

sensitivities by their inverse distance to the point of interest, as suggested by Garcìa and Steven for stress computation [13]. Thus, the compound weighting factor, w_i for each sampled sensitivity value, i used for the weighted least squares fit is defined as:

$$w_i = \alpha_i / \left| x_p - x_i \right| \tag{12}$$

where $|x_p - x_i|$ is a measure of the distance between the boundary point, x_p and the location of the sampled sensitivity value, x_i.

Sensivities can be sampled either at element centers, Fig. 2 or at the four Gauss integration points, Fig. 3 for the plane four-node bilinear element, usually employed for boundary based structural optimization [1,6,11]. These schemes are investigated through numerical examples in the following sections.

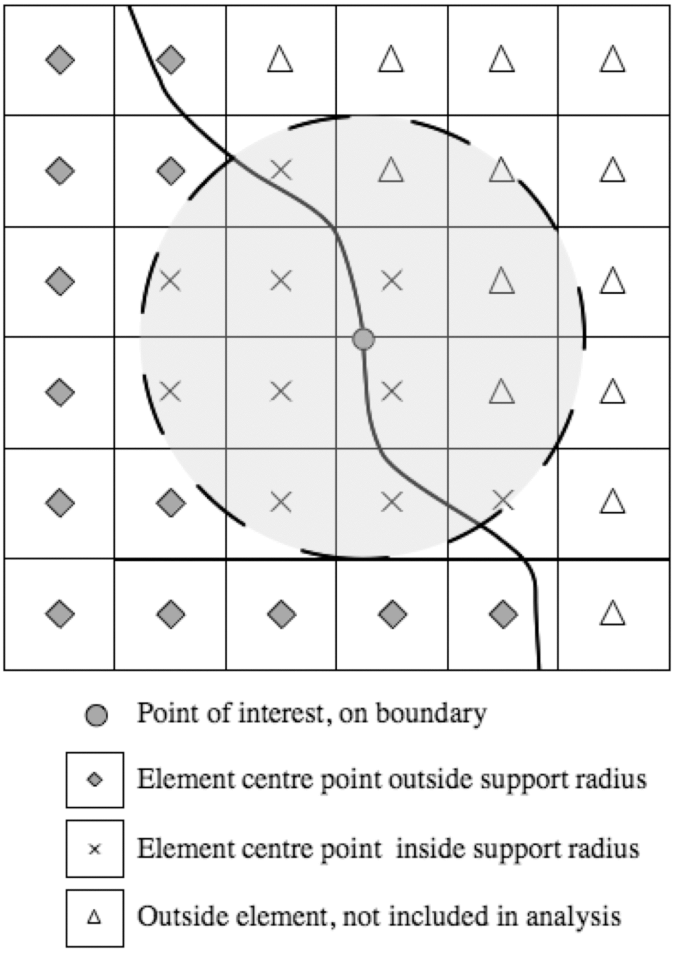

Fig. 2. Element center point sampling scheme for least squares method

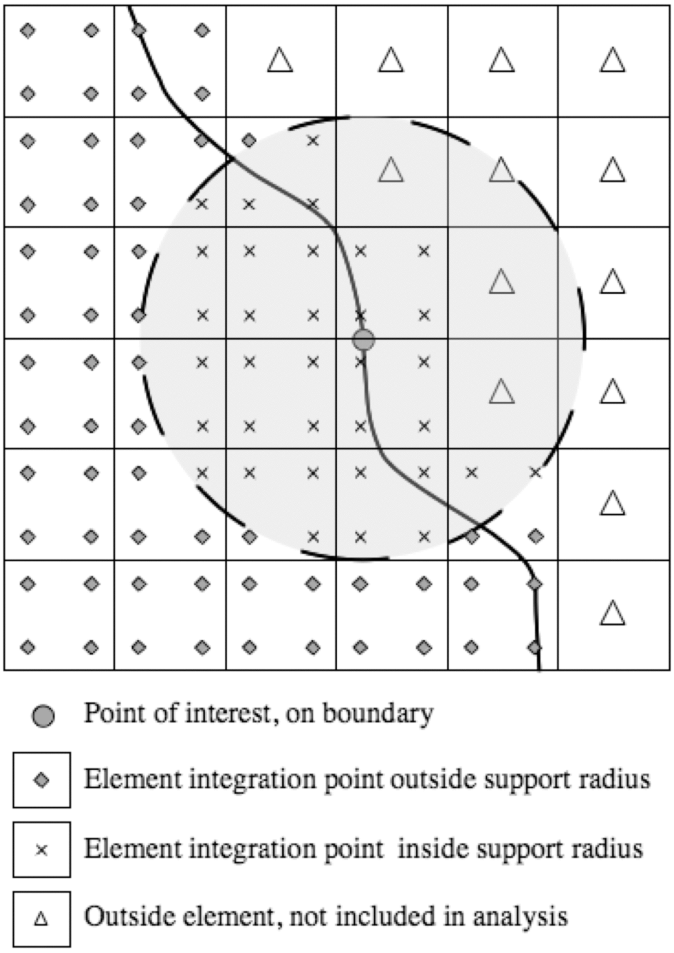

Fig. 3. Element Gauss integration point sampling scheme for least squares method

4.3 Hole in plate

The first example is a square plate with central circular hole, which is subject to a uniform tensile load. Due to symmetry conditions only one quarter of the structure is analysed. The fixed mesh is composed of 30 × 30 unit sized square elements, Fig. 4a, and the equivalent fitted mesh is shown in Fig. 4b. The structure material has a Young's

modulus of 1.0 and Poisson's ratio of 0.3. Normalized velocities are computed around the edge of the hole.

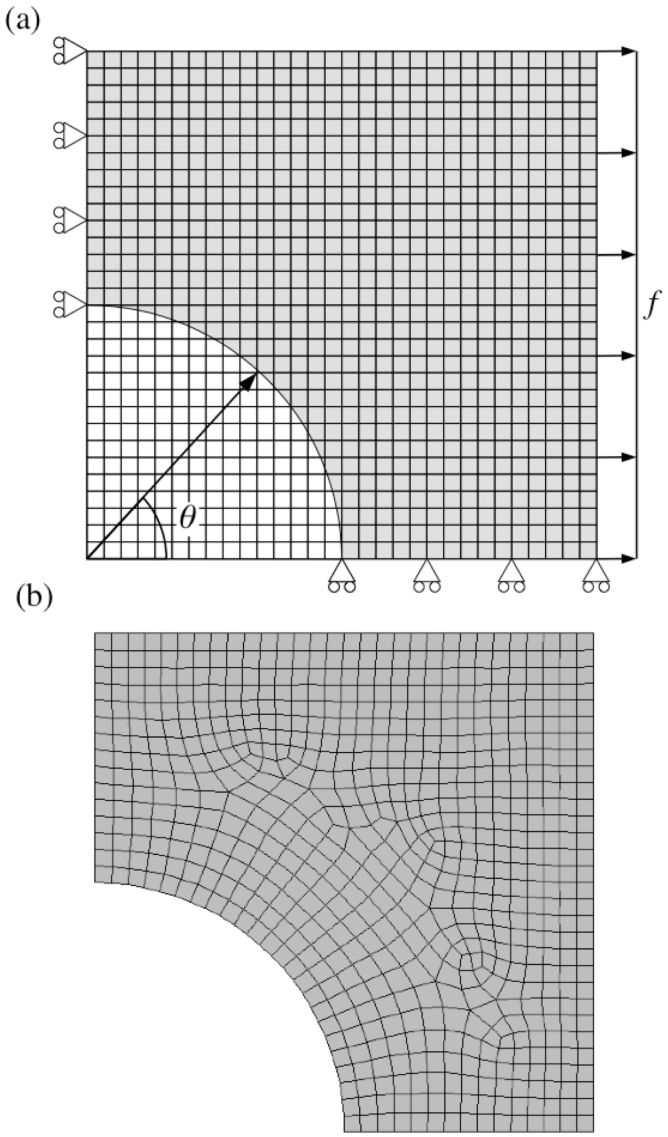

Fig. 4. Hole in plate example: (a) fixed mesh and boundary conditions; (b) equivalent fitted mesh

First, boundary velocities are computed using the AFG method with the two nodal averaging techniques, Fig. 5. The area-fraction weighted averaging produces less

spurious fluctuations, when compared to the simple averaging method. This suggests that weighting sensitivity values by area-fraction is beneficial, even for the nodal averaging technique. However, both nodal average methods are not smooth when compared with the solution obtained from the fitted mesh analysis.

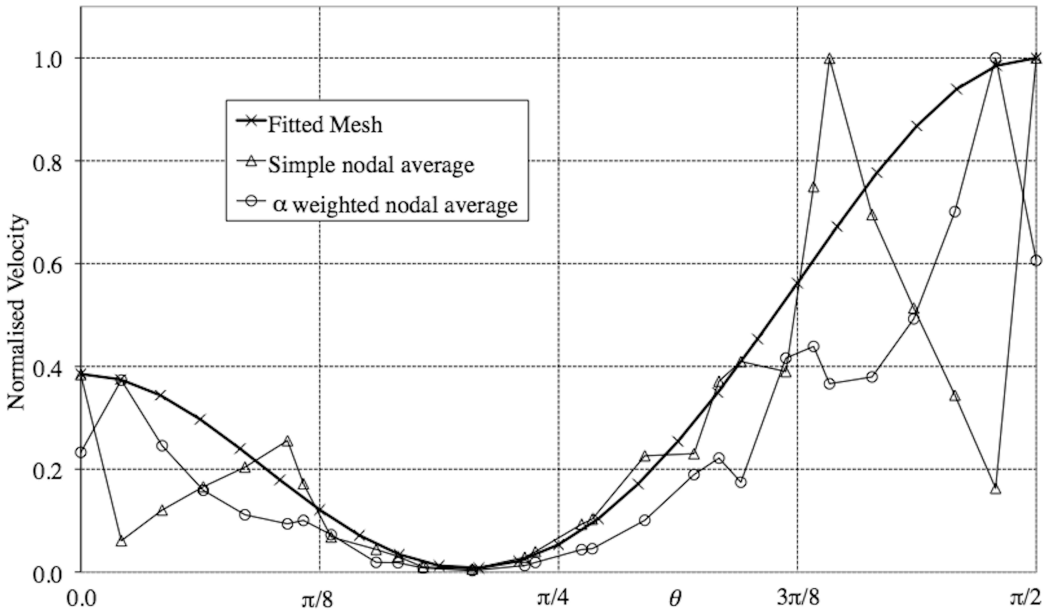

Fig. 5. Hole in plate normalized velocity distribution using nodal averaging

The weighted least squares method is applied to compute the normalized velocity distributions with sampling at the element centers (Fig. 6) and at the four integration points (Fig. 7). Both figures show that the weighted least squares method produces a superior relative accuracy of velocity distribution than the nodal averaging method, Fig. 5. For both sampling schemes, increasing the support radius obtains better relative accuracy as expected, and comparing figures reveals little difference between the two sampling schemes. The large error at $\theta = 0$ for the center point sampling, Fig. 6, is caused by an ill-conditioned matrix when solving the least squares problem, as there are too few

points within the support radius. When using a least squares approach to compute sensitivities in optimization, care should be taken to ensure a well-conditioned matrix by including more points if necessary.

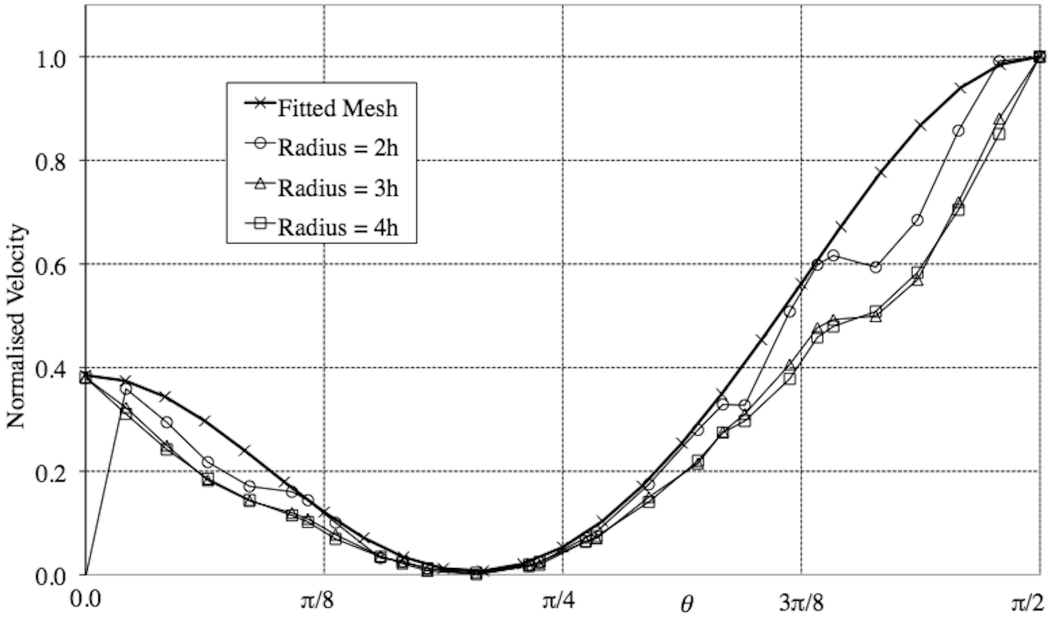

Fig. 6. Hole in plate normalized velocity distribution using weight least squares method with sampling at element centers

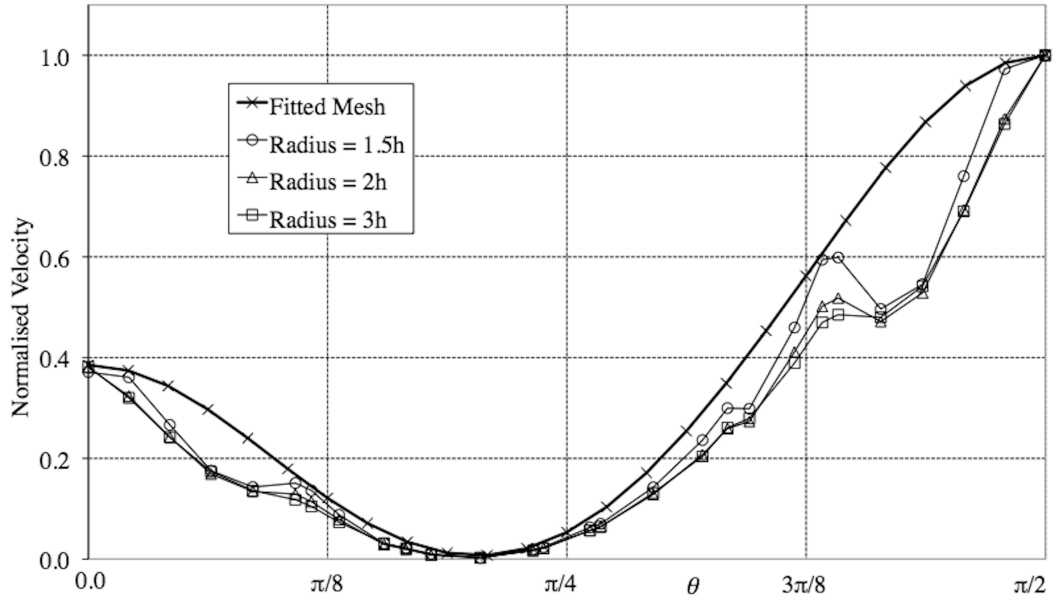

Fig. 7. Hole in plate normalized velocity distribution using weight least squares method with sampling at the four integration points

4.4 Truss example

The second example is a simple truss-type structure modeled as a continuum. The fixed mesh is composed of 28 × 18 square elements with edge length h=0.5, Fig. 8a, and the equivalent fitted mesh is shown in Fig. 8b. The material has a Young's modulus of 1.0 and Poisson's ratio of 0.3. Normalized velocities are computed along edge 1 of the truss, as indicated in Fig. 8a.

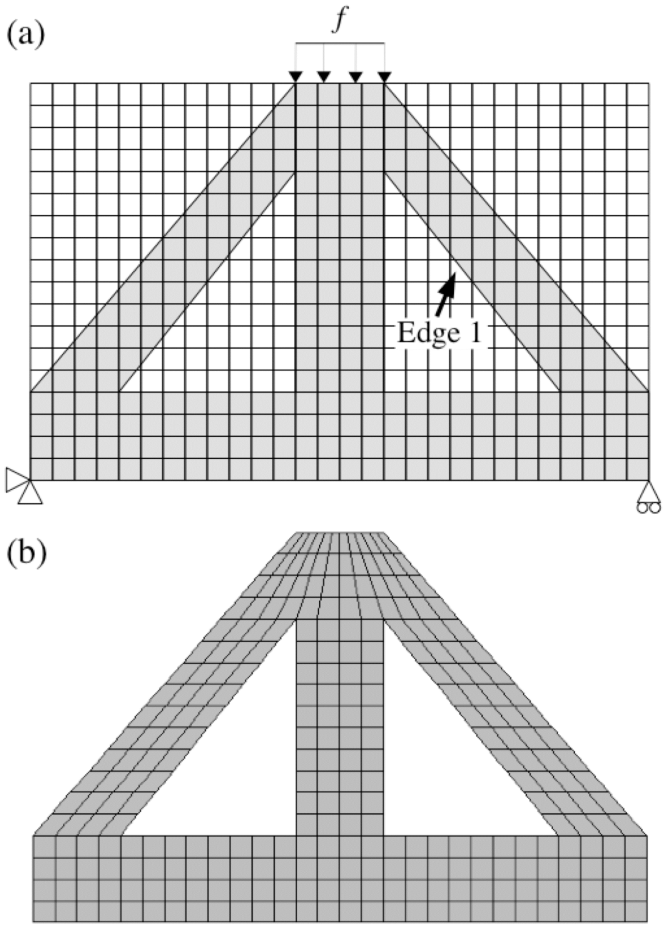

Fig 8. Truss example: (a) fixed mesh and boundary conditions; (b) equivalent fitted mesh

Normalized velocity distributions are computed using the proposed weighted least squares scheme with sampling at the elemental centers, Fig. 9 and at the four integration points, Fig. 10. In contrast to the previous example, increasing the support radius does not improve the velocity distribution for either sampling scheme. This is because the sensitivities at the top of edge 1 are influenced by the sensitivities sampled in the central strut as the radius is increased. Thus, increasing the support radius does not improve relative accuracy of the sensitivities for all problems. The results obtained using the integration point sampling scheme, Fig. 10, appear closer to the fitted mesh reference solution, compared to solutions computed using the central point scheme, Fig.9. Thus it may be concluded that the sampling scheme at the four point integration with a small to moderate support radius would yield a reliable sensitivity computation for boundary based structural optimization. This trend has been confirmed by a variety of numerical examples, although not presented here for brevity.

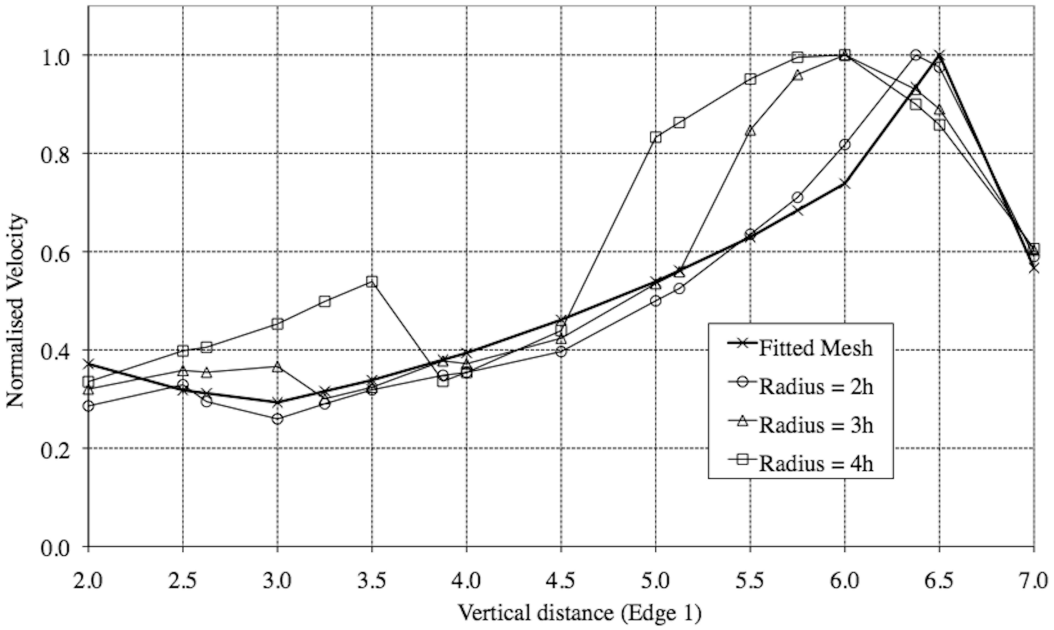

Fig. 9. Truss edge 1 normalized velocity distribution using weight least squares method with sampling at element centers

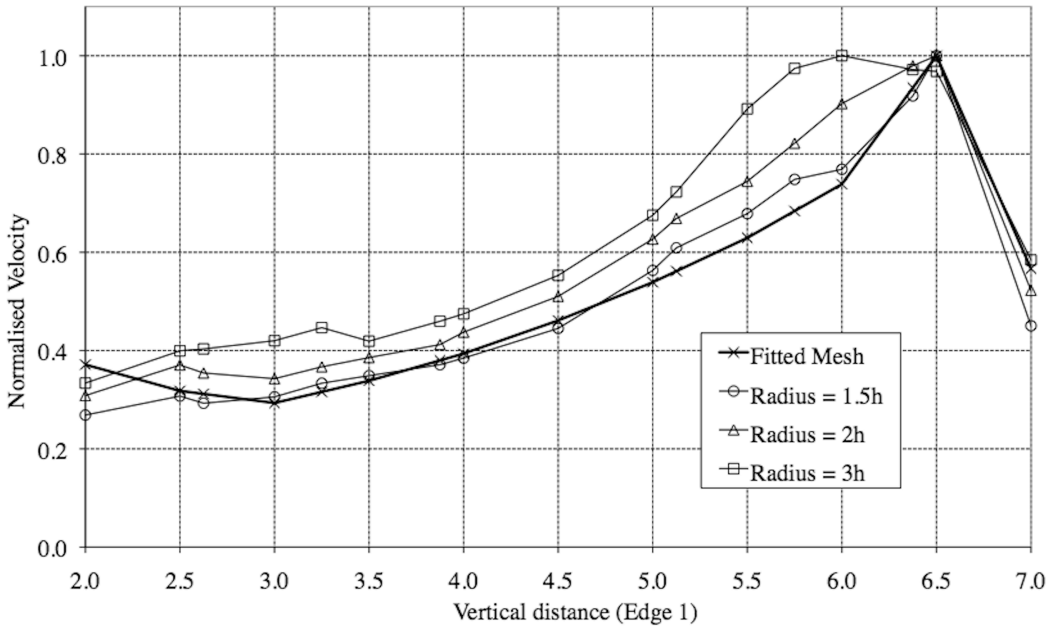

Fig. 10. Truss edge 1 normalized velocity distribution using weight least squares method with sampling at the four integration points

4.5 Discussion

Our observations show that the results for the AFG method using the weighted least squares method consistently demonstrates superior results in relative accuracy of boundary velocity distribution compared to the nodal averaged results. However, the choice of parameters used for the least squares method can significantly affect the solution. Whilst a greater support radius can improve the relative accuracy, it can also reduce the accuracy by including sampled sensitivities from parts of the structure not immediately connected with the point of interest. Experience suggests a support radius of $3h$ for center point and $2h$ for the four point sampling scheme is suitable for most

problems. Thus, we employ the weighted least squares method for the four integration point sampling scheme using a second order basis function and support radius of $2h$ for the sensitivity computation in the optimization method presented in the next section.

The proposed weighted least squares method has been implemented and investigated for two-dimensional structures. However, the proposed approach can be easily extended for three-dimensional applications by computing sensitivity values at the gauss points of the 3-d element and using a 3-d second order basis function for the least squares fit:

$$\varsigma(x,y,z) = c_0 + c_1 x + c_2 y + c_3 z + c_4 xy + c_5 xz + c_6 yz + c_7 x^2 + c_8 y^2 + c_9 z^2 \qquad (13)$$

5. Level set method implementation

This section presents details of an efficient and stable numerical implementation of a level set based structural optimization method. The method is implemented to solve the minimization of compliance problem Eq. (2). The initial structure is defined as a signed distance implicit function, Eq. (1) that is discretized at nodes of a regular grid of square elements and interpolated using bilinear shape functions. For convenience, the same grid is used for the fixed grid FE mesh.

The implicit function is updated iteratively through Eq. (7) using the velocity function defined by Eq. (6). The boundary sensitivity values are computed using the numerical scheme identified in Section 4. When defining the time step in Eq. (8) a reasonably conservative value is chosen, β=0.5, to ensure stability throughout the optimization process.

5.1 Volume constraint

The volume constraint for the compliance problem, Eq. (2) is enforced by the constant, λ when computing the velocity function, Eq. (6). The value of λ is defined so that the solution remains feasible, or at least moves towards the feasible region. We employ a volume conserving λ value calculated at each iteration using Newton's method. We find this to work well as volume change is observed to be usually approximately linear to λ.

Change in volume is calculated by integrating the velocity function, Eq. (6) over the free boundary:

$$\Delta Vol(\lambda) = \Delta t \int_{\Gamma_0} \lambda - \varsigma(u) d\Gamma_0 \qquad (14)$$

where $\Delta Vol(\lambda)$ is the reduction in structure volume for a given λ value. A numerical estimate of this boundary integral provides a tool to compute, with reasonable accuracy, the change in volume for a given value of λ. A good initial guess for λ^0 was found to be the λ value computed for the previous level set iteration. If the initial volume change ΔVol^0 is within tolerance of the target volume change ΔVol^t then no further iterations are required. Otherwise, a second guess is constructed by comparing ΔVol^0 and ΔVol^t. If $\Delta Vol^0 < \Delta Vol^t$, then $\lambda^1 = 2\lambda^0$, otherwise, $\lambda^1 = 0.5\lambda^0$ and the iteration is continued using Newton's method to find a λ value that produces a volume change within 1% of the target volume.

The target volume is set to the difference between current and constraint values: $\Delta Vol^t = Vol^k - Vol^*$. However, if the volume is far from the constraint then the target may not be achievable under the CFL condition. Thus, an upper limit is defined in terms of the

free boundary length: $|Vol^t|_{\max} = 0.1h\,|\Gamma_0|$. This value is chosen from experience to ensure a reasonably smooth progression of the structure whose volume is far from the constraint.

5.2 Extension velocity

So far the velocity function defined in Eq. (6) is only computed at points along the structural boundary. In order to update the level set function using Eq. (7), velocity values, $V_{n,i}$ are required at all grid nodes, i. Thus, the velocity function must be extended or extrapolated to grid points away from the boundary. Natural velocity extension schemes compute strain and sensitivity fields over the entire design domain. Methods that achieve this include filling the void part with a fictitious weak material [1,12], or smoothing the velocity field over the discontinuity at the boundary edge [6]. However, the implicit function often becomes too steep or flat around the boundary, which leads to potential stability issues. Thus, these schemes usually require frequent reinitializing of the implicit function to a signed distance function to maintain stability [1,6].

To avoid frequent reinitialization, we employ an extension velocity technique designed to maintain the signed distance function [16]. This technique ensures the preservation of the signed distance by using the efficient fast marching method to solve the following equation:

$$\nabla\varphi_t \nabla V_{ext} = 0 \qquad (15)$$

where φ_t is a temporary signed distance implicit function and V_{ext} is the extended velocity function. The extended velocity function is constrained to maintain the values already computed along the boundary.

5.3 Reinitialization

In practice, velocities are only extended to nodes within a local region of the boundary, usually called a narrow band [17]. This approach improves efficiency, as velocity computation and implicit function update are restricted to a portion of grid nodes and the signed distance function is only maintained for these nodes. A local region "band-width" of 4 grid lengths, h either side of the boundary was chosen to give reasonable computational efficiency. This local region is fixed until the boundary approaches its limits, when a new narrow band region is defined and the implicit function is reinitialized to a signed distance function over the entire domain.

The reinitialization approach adopted in this work is to use the fast marching method to solve the eikonal equation [16]:

$$\left|\nabla \varphi_t\right| = 1 \tag{16}$$

The starting point of this approach is the zero level set, which is explicitly maintained during reinitialization. The fast marching method is run separately for nodes inside and outside the structure. The initial signed distance values for nodes within h of the zero level set are computed using distances to neighboring intersections of grid lines and the zero level set [16] and used as a starting point for the fast marching method. A similar process is used to compute the temporary signed distance implicit function when computing extension velocities, Eq. (16).

5.4 Gradient computation

The upwind finite difference scheme for gradient calculation is often employed by level set methods due to its favorable stability. This scheme uses either forward or

backward differences to compute gradient components depending on direction of movement [17]. However, using first order differences can lead to poor gradient estimation and numerical instability. Therefore, we employ the more accurate, higher order WENO (Weighted Essentially Non-Oscillatory) scheme to compute gradient components [18]. This scheme constructs three polynomials from surrounding implicit function values to gain three gradient estimates. These gradients are weighted by estimates on polynomial smoothness and averaged to produce an overall gradient estimation. This approach can avoid discontinuities in the implicit function when estimating gradients and helps prevent noise being generated in the solution.

5.5 Convergence criterion

The convergence criterion is computed if the volume constraint is satisfied and is defined using the maximum change in compliance over the previous 5 iterations:

$$\Delta C^k = \max\left(\left| C^k - C^m \right| / C^k \right), \quad m \in [k-5, k-1] \tag{17}$$

where C^k is the compliance computed at iteration k and the optimization process is terminated if $\Delta C^k < 0.001$.

6. Optimization examples

6.1 Cantilever beam example

The first example is a simple cantilever beam with aspect ratio 2:1, Fig. 11a. The beam is discretized using 160 × 80 unit square elements and the material properties are E=1.0, v=0.3. The volume constraint for the minimization of compliance problem, Eq. (2)

is set to 50% of the entire design domain. The structure converges to an optimum solution after only 58 iterations, Fig. 11b with a compliance value of 60.1, Fig. 12.

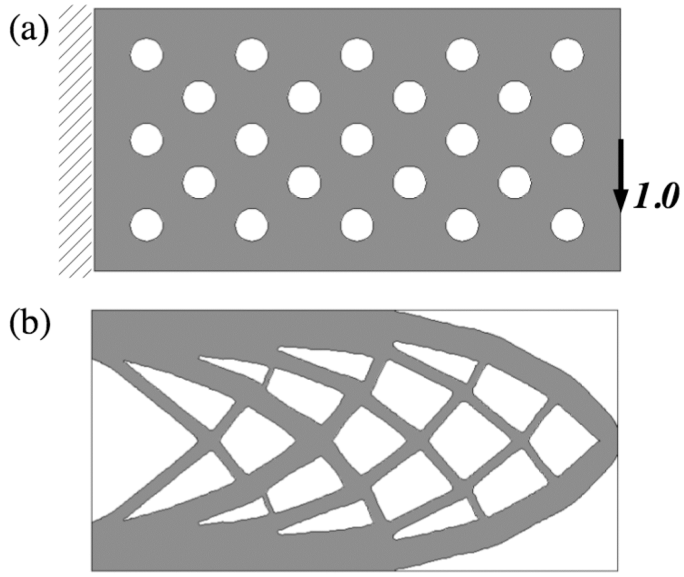

Fig. 11. Cantilever example: (a) initial design and boundary conditions; (b) final solution

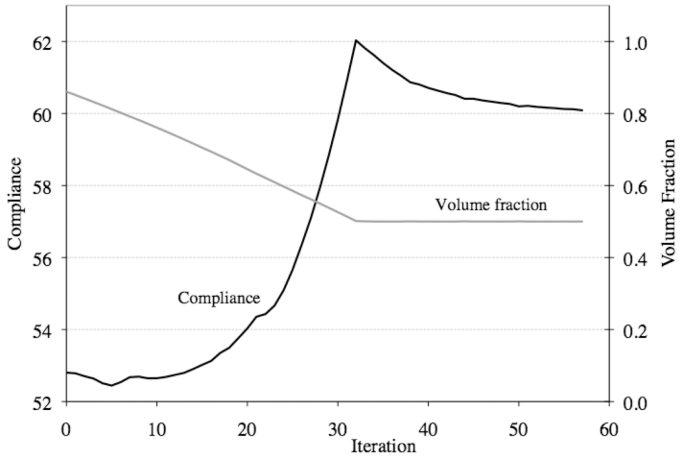

Fig. 12. Convergence history of the cantilever example

6.2 MBB beam example

The second example is an MBB beam [8], which has material properties of E=1.0, v=0.3. Due to symmetry about the vertical axis, only the right half of the beam is

modeled, Fig. 13a, which is discretized using 120 × 40 square unit elements. The volume constraint is set to 45% of the entire design domain. A converged solution is obtained after 47 iterations, Fig. 13b with a compliance value of 198.1, Fig. 14.

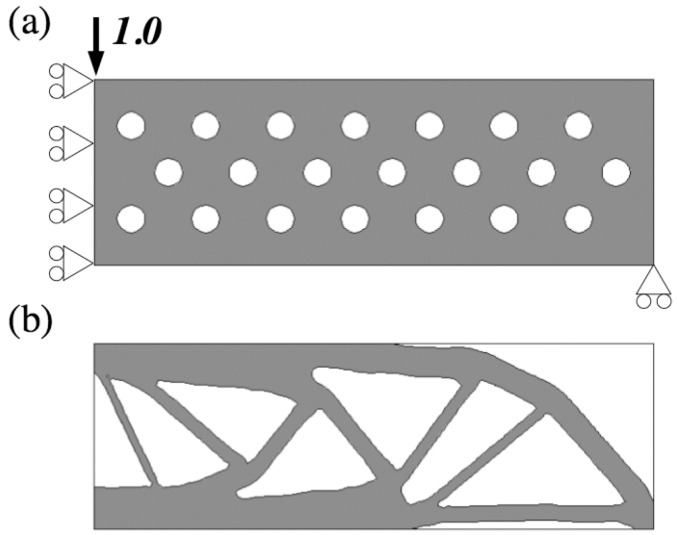

Fig.13. MBB beam example: (a) initial design and boundary conditions; (b) final solution

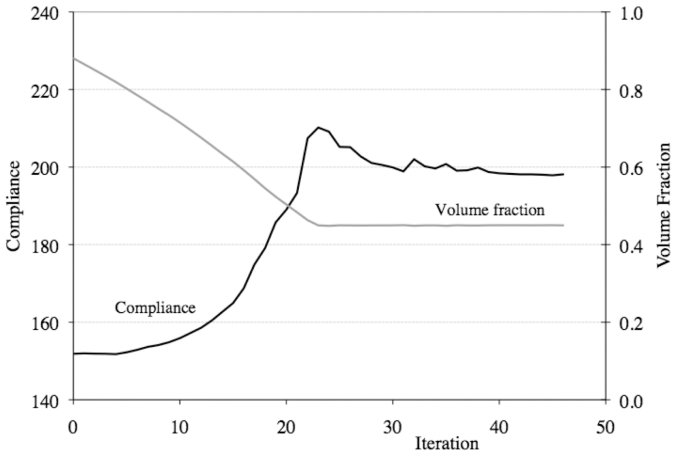

Fig. 14. Convergence history of the MBB beam example

6.3 Discussion

The optimization examples demonstrate that optimum solutions can be reliably achieved using the simple and efficient AFG method with the proposed weighted least

squares scheme for sensitivity computation. Solutions are obtained in a small number of iterations and did not require any smoothing or regularizing of the velocity function. This suggests that the relative distribution of sensitivity values computed throughout the optimization process is of sufficient accuracy and numerical instabilities are not significant.

7. Conclusions

It has been established that structural sensitivities computed by the AFG FEM for compliance minimization can produce spurious local fluctuations. These errors in the relative accuracy can destabilize boundary-based optimization over successive iterations, leading to non-convergence or a non-optimal solution. Our investigation shows that the errors in sensitivity computation are primarily governed by area-fraction values, although it is also dependent on the approximated geometry, loading conditions and sometimes Poisson's ratio. We propose a weighted least squares method with a weighting function based on area-fraction and the distance of the sampling point to the boundary. This achieves a reliable sensitivity computation for optimization using the four integration point sampling scheme with a second order basis function and support radius of $2h$ for a wide range of problems.

The sensitivity computation scheme is demonstrated using level set based topology optimization. For this study, we present an implementation of the level set method with stable numerical properties. The numerical examples show fast and reliable convergence to optimum solutions of classical benchmark problems in topology optimization. This demonstrates that the proposed weighted least squares scheme

combined with the simple and efficient AFG method can be used to compute sufficiently accurate sensitivities for boundary based optimization without additional regularization.

Acknowledgements

The work reported in this paper has been undertaken as part of the Innovative Design and Manufacturing Research Centre at the University of Bath, funded by the Engineering and Physical Sciences Research Council (EPSRC). The authors would like to thank Numerical Analysis Group at the Rutherford Appleton Laboratory for their FORTRAN HSL packages.

References

[1] G. Allaire, F. Jouve, A.M. Toader, Structural optimization using sensitivity analysis and a level-set method. J. Comp. Phys. 194 (2004) 363-393.

[2] G-W. Jang, Y.Y Kim, K.K. Choi, Remesh-free shape optimization using the wavelet-Galerkin method. Int. J. Solids Struct. 41 (2004) 6465-6483.

[3] S. Lee, B.M. Kwak, Smooth boundary topology optimization for eigenvalue performance and its application to the design of a flexural stage. Eng. Optim. 40 (2008) 271-285.

[4] H. Kim, O.M. Querin, G.P. Steven, Y.M. Xie, Improving efficiency of evolutionary structural optimization by implementing fixed grid mesh. Struct. Multidiscip. Optim. 24 (2003) 441-448.

[5] S. Y. Woon, O.M. Querin, G.P. Steven, On improving the GA step-wise shape optimization method through the application of the Fixed Grid FEA paradigm. Struct. Multidiscip. Optim. 25 (2003) 270-278.

[6] S. Wang, M.Y. Wang, A moving superimposed finite element method for structural topology optimization. Int. J. Numer. Methods Eng. 65 (2006) 1892-1922.

[7] L. Van Miegroet, P. Duysinx, Stress concentration minimization of 2D filets using X-FEM and level set description. Struct. Multidiscip. Optim. 33 (2007) 425-438.

[8] M.Y. Wang, X. Wang, D. Guo, A level set method for structural topology optimization. Comput. Methods Appl. Mech. Eng. 192 (2003) 227-246.

[9] T. Belytschko, S.P. Xiao, C. Parimi, Topology optimization with implicit functions and regularization. Int. J. Numer. Methods Eng. 57 (2003) 1177-1196.

[10] C.S. Edwards, H.A. Kim, C.J. Budd, Smooth Boundary Based Optimisation Using Fixed Grid, in: Proceedings of 7th World Congress on Structural and Multidisciplinary Optimization, Seoul, Korea, 2007, pp. 1789-1798.

[11] S.Y. Wang, K.M. Lim, B.C. Khoo, M.Y. Wang, An extended level set method for shape and topology optimization. J. Comp. Phys. 221 (2007) 395-421.

[12] J. Luo, Z. Luo, L. Chen, L. Tong, M.Y. Wang, A semi-implicit level set method for structural shape and topology optimization. J. Comp. Phys. 227 (2008) 5561-5581.

[13] M.J. Garcìa, G.P. Steven, Fixed grid finite elements in elasticity problems. Eng. Comput. 16 (1999) 145–164.

[14] N.H. Kim, Y. Chang, Eulerian shape design sensitivity analysis and optimization with a fixed grid. Comput. Methods Appl. Mech. Eng. 194 (2005) 3291-3314.

[15] R.D. Cook, D.S. Malkus, M.E. Plesha, R.J. Witt, Concepts and applications of finite element analysis, fourth ed., John Wiley & Sons, Inc., USA, 2002.

[16] D. Adalsteinsson, J.A. Sethian, The fast construction of extension velocities in level set methods. J. Comp. Phys. 148 (1999) 2-22.

[17] J.A. Sethian, Level set methods and fast marching methods, second ed., Cambridge University Press, New York, 1999.

[18] G-S. Jiang, D. Peng, Weighted ENO schemes for Hamilton-Jacobi equations. SIAM J. Sci. Comput. 21 (2000) 2126-2143.